

## *Supporting Information*

Effect of zeolite confinement on the conversion of 1-butanol to butene isomers: mechanistic insights from DFT based microkinetic modelling

Mathew John, Konstantinos Alexopoulos, Marie-Françoise Reyniers\* and Guy B. Marin

*Laboratory for Chemical Technology, Ghent University, Technologiepark 914, B-9052 Ghent, Belgium*

\* Corresponding author.

Tel.: +32 9 331 1735. Fax: +32 9 331 1759. E-mail: [MarieFrancoise.Reyniers@ugent.be](mailto:MarieFrancoise.Reyniers@ugent.be)

### **Contents**

The Supporting Information includes Al siting in H-FER zeolite (Figure S1) and the Arrhenius activation energies and pre-exponential factors, forward reaction rate coefficients and equilibrium coefficients for elementary steps associated with conversion of 1-butanol to DBE, 1-butene and isobutene in H-FER-T2 as tabulated in Table S1. TS geometry (Figure S2), thermodynamic and kinetic parameters (Table S2) for direct formation of 2c-butene from butanol dimer in H-FER-T1b is presented. It also includes, geometric parameters for TS-12 in different zeolites (Figure S3), stability of adsorbed butanol dimer and di1-butyl ether in zeolite (Table S3) and their dispersive and non-dispersive interaction (Table S4), thermodynamic cycle (Table S5 and S6 for ether formation via TS-7 and 2t-butene formation from 1-butanol dimer via TS-12), comparison of previously reported simulations for dehydration of 1-butanol to 1-butene<sup>14</sup> and that obtained in the present study at 450K (Figure S5) and 500K (Figure S6) and pressure dependency for 2-butene formation reactions.

### Al siting in H-FER zeolite:

There are different distinct tetrahedral sites in the FER framework<sup>1</sup> (see Figure S1) and the Al distribution can vary depending upon the synthesis procedure<sup>2,3</sup>. Amongst them, T1b and T2 site are reported to be the most preferred location of Al in H-FER<sup>3,4</sup>. A detailed study is performed for H-FER with Al at the T1b site (FER-T1b) as Al at this site is most abundant in commercially available H-FER from Zeolyst<sup>3,4</sup>. On the other hand, H-FER with Al at the T2 site (FER-T2) may also be of importance and has been used for several theoretical studies<sup>5-9</sup>.

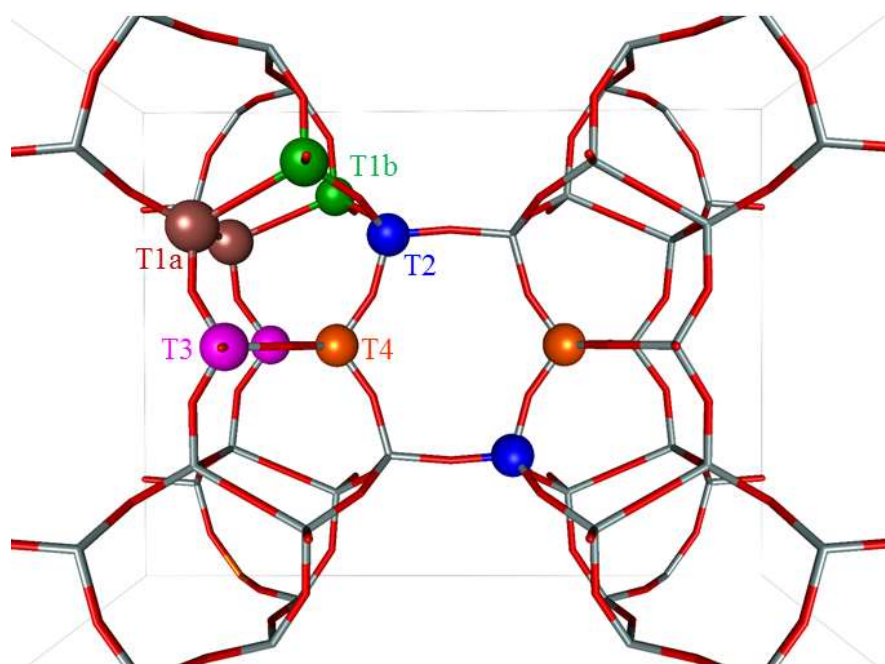


**Figure S1.** The tetrahedral positions for location of Al atom in FER framework.

Arrhenius activation energies and pre-exponential factors, forward reaction rate coefficients and equilibrium coefficients for elementary steps associated with conversion of 1-butanol to DBE, 1-butene and isobutene in H-FER-T2 are tabulated in Table S1.

**Table S1.** Standard reaction enthalpy (kJ/mol), reaction entropy (J/mol/K), activation energy (kJ/mol), pre-exponential factor ( $s^{-1}$ ), forward reaction rate coefficient  $k_f$  ( $s^{-1}$ ) at 500 K and equilibrium coefficient at 500 K ( $10^{-2}$  kPa $^{-1}$ ,  $10^2$  kPa or dimensionless for adsorption, desorption and surface transformation, respectively) for the elementary steps (numbered as indicated in Figure 1) in H-FER -T2.

	<b>Elementary steps</b>	$\Delta H_r^0$	$\Delta S_r^0$	$E_{a(f)}$	$A_f$	$k_f(500K)$	$K_{eq}(500K)^{\#}$
1	1-BuOH(g) + * $\leftrightarrow$ M1	-148	-199	—	—	—	1.1E+05
6	M1 $\leftrightarrow$ M2	43	-14	—	—	—	6.2E-06
7	M2 $\leftrightarrow$ 1-Butene* + H2O(g)	52	255	75	2.5E+15	3.7E+07	8.2E+07
8	1-Butene* $\leftrightarrow$ 1-Butene(g) + *	96	109	—	—	—	4.7E-05
9	M2 $\leftrightarrow$ Butoxy + H2O(g)	35	167	87	4.0E+14	3.6E+05	1.4E+05
10	Butoxy $\leftrightarrow$ 1-Butene*	17	88	123	1.6E+13	2.0E+00	6.0E+02
11	M1 + BuOH(g) $\leftrightarrow$ D1	-137	-182	—	—	—	6.7E+04
12	D1 $\leftrightarrow$ D2	55	7	—	—	—	3.9E-06
15	D2 $\leftrightarrow$ DBE* + H2O(g)	10	151	86	9.4E+12	9.7E+03	8.6E+06
16	DBE* $\leftrightarrow$ DBE(g) + *	197	210	—	—	—	3.1E-11
20	DBE* $\leftrightarrow$ C4	104	37	158	1.8E+13	5.2E-04	1.2E-09
21	C4 $\leftrightarrow$ 1-Butene*+ BuOH(g)	66	235	—	—	—	2.1E+05
28	1-butene* $\leftrightarrow$ 2-butoxy	-18	-90	57	3.2E+09	3.5E+03	1.6E-03
32	2-butoxy $\leftrightarrow$ iso-butoxy	16	-7	124	3.3E+14	3.7E+01	8.8E-03
33	iso-butoxy $\leftrightarrow$ iso-butene*	2	33	106	6.1E+13	5.5E+02	3.3E+01
34	iso-butene* $\leftrightarrow$ iso-butene(g)+ *	77	172	—	—	—	1.1E+00

$\#$  elementary steps involving adsorption/ desorption corrected using NIST experimental data

Direct formation of 2c-butene from butanol dimer in H-FER-T1b:

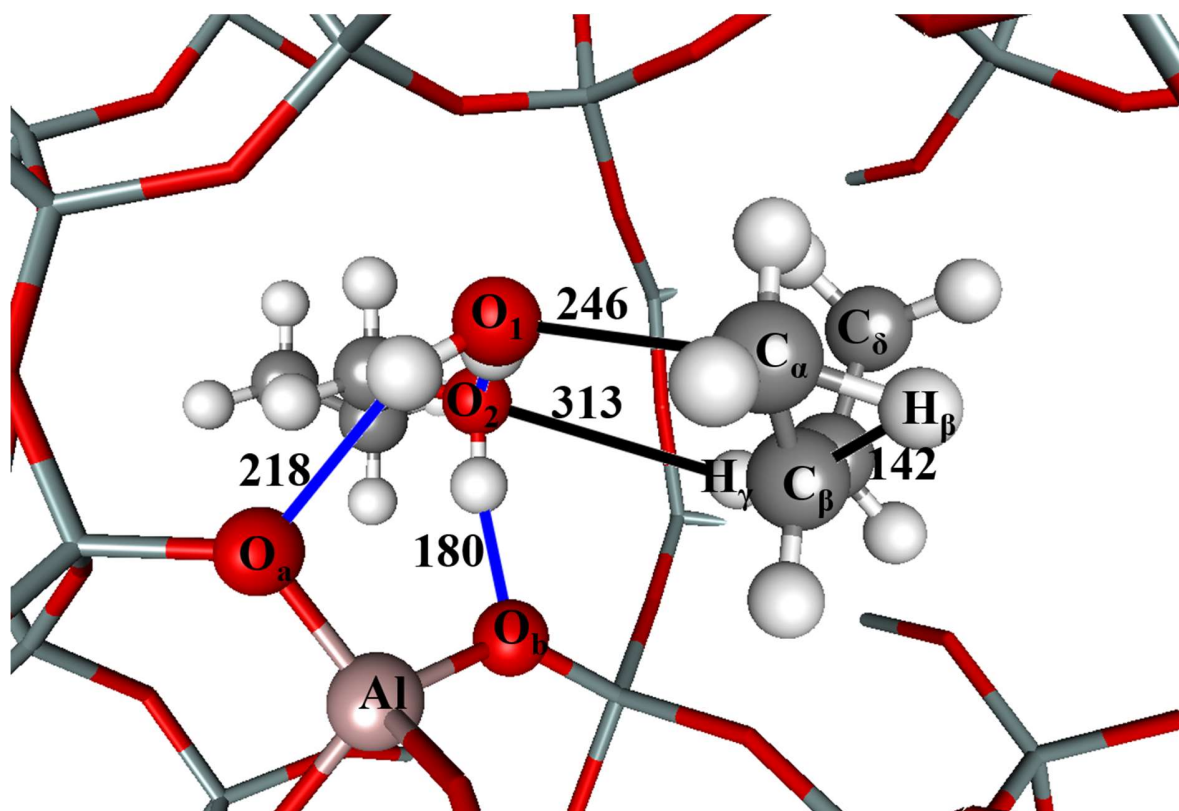


**Figure S2.** Transition state geometry for formation of 2c-butene from butanol dimer (D1) in H-FER-T1b.

**Table S2.** Standard reaction enthalpy (kJ/mol), reaction entropy (J/mol/K), activation energy (kJ/mol), pre-exponential factor ( $s^{-1}$ ), forward reaction rate coefficient  $k_f$  ( $s^{-1}$ ) at 500 K and equilibrium coefficient at 500 K ( $10^2$  kPa) for formation of 2c-butene from butanol dimer (D1) in H-FER-T1b.

Elementary step	$\Delta H_r^\circ$	$\Delta S_r^\circ$	$E_{a(f)}$	$A_f$	$k_f(500K)$	$K_{eq}(500K)^\#$
35 D1 $\leftrightarrow$ C2+2-c-butene(g)	77	210	167	$2.4 \cdot 10^{15}$	$8.1 \cdot 10^{-3}$	$9.4 \cdot 10^1$

$\#$  elementary step involving adsorption/desorption corrected using NIST experimental data

**Transition state structure for TS-12 in H-ZSM-5, H-ZSM-22 and H-FER**

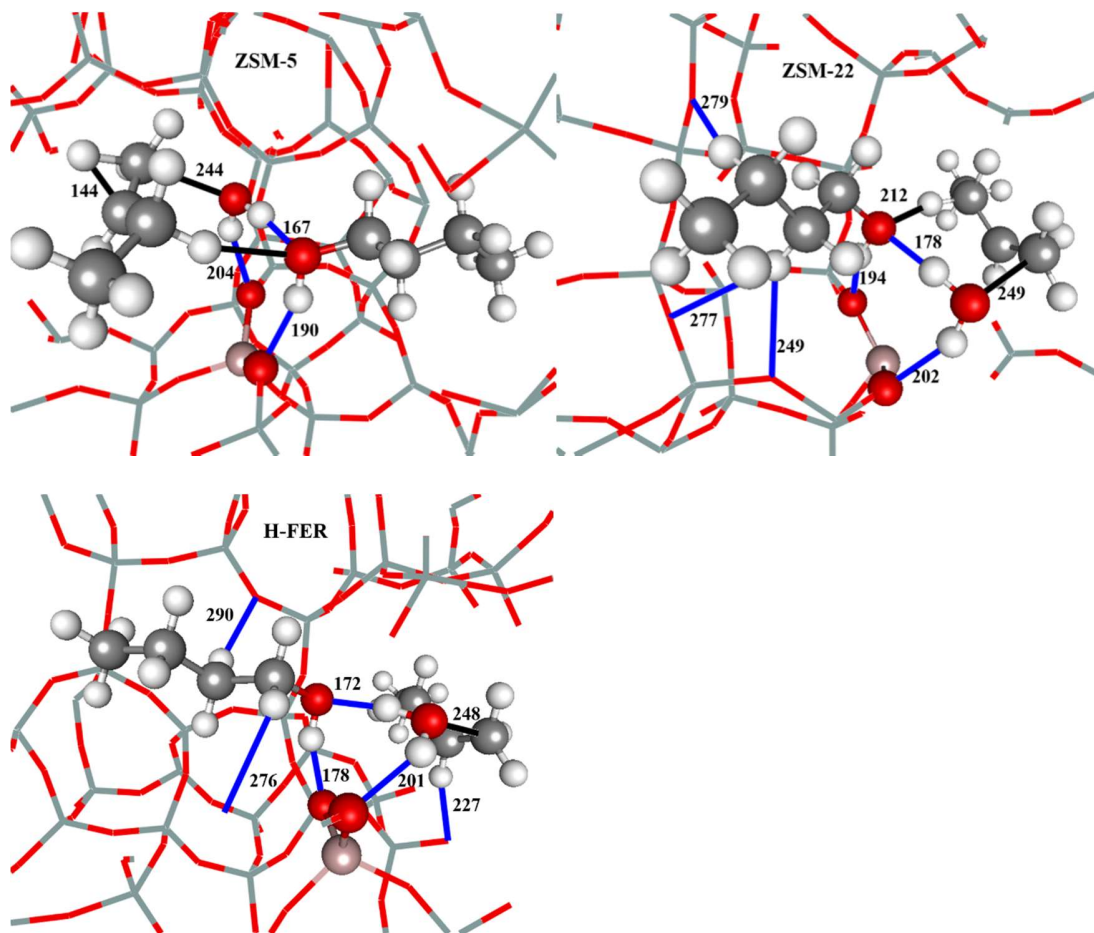


**Figure S3 :** Transition state structure TS-12 in H-ZSM-5, H-ZSM-22 and H-FER. Selected diatomic distances  $\leq 300$  pm are indicated.

**Table S3:** Thermodynamics for the adsorption of 1-butanol dimer and di-1-butyl ether in different zeolites.

Zeolite	1-butanol dimer adsorption energy $\Delta$ (D1-[ZeoH+2*BuOH])			Di-1-butyl ether adsorption energy $\Delta$ (DBE*-[ZeoH+DBE])		
	$\Delta H_{ads}^0$	$\Delta S_{ads}^0$	$\Delta G_{ads}^0$	$\Delta H_{ads}^0$	$\Delta S_{ads}^0$	$\Delta G_{ads}^0$
	kJ/mol	J/mol/K	kJ/mol	kJ/mol	kJ/mol	kJ/mol
<b>H-ZSM-5</b>	-272	-375	-84	-191	-209	-86
<b>H-ZSM-22</b>	-274	-380	-84	-195	-222	-84
<b>H-FER</b>	-242	-400	-42	-137	-233	-20

**Table S4:** Dispersive and non-dispersive interaction of adsorbed butanol dimer (D1) and di-1-butyl ether (DBE\*) in different zeolites with respect to gas phase molecule 1 and unloaded zeolite

Zeolite	1-butanol dimer adsorption energy $\Delta$ (D1-[ZeoH+2*BuOH])			Di-1-butyl ether adsorption energy $\Delta$ (DBE*-[ZeoH+DBE])		
	DFT-D2	DFT	Dispersion	DFT-D2	DFT	Dispersion
	kJ/mol	kJ/mol	kJ/mol	kJ/mol	kJ/mol	kJ/mol
<b>H-ZSM-5</b>	-283.2	-110.1	-173.2	-195.8	-57.1	-138.7
<b>H-ZSM-22</b>	-287.9	-107.7	-180.2	-203.3	-53.7	-149.6
<b>H-FER</b>	-258.8	-38.4	-220.4	-148.8	41.3	-190.1

## Thermodynamic cycle

The zeolite acid strength and confinement effect have a significant influence on the reaction rates. A thermodynamic cycle provides a useful link between adsorption/activation energy with the inherent properties of the catalyst and reacting species such as acid strength and protonation affinity. Thus, it allows comparison between different adsorbed/transition state structures based on stabilizing and destabilizing contributions.

The thermodynamic cycle is explained considering as an example ether formation from butanol dimer via SN2 reaction ( $D1 \rightarrow DBE^*$ , via TS7). As reported previously<sup>14</sup>, the pre-exponential factor does not vary significantly for this ether formation reaction, allowing to draw important conclusions based on the enthalpic contributions. Since the enthalpy term depends mainly on the 0 K electronic energy obtained from the DFT calculations, the 0 K values are used in the following analysis. The thermodynamic cycle for adsorption of 1-butanol in the zeolite forming butanol dimer and its further conversion to ether via TS7 (SN2 type substitution reaction) is shown in Figure S4.

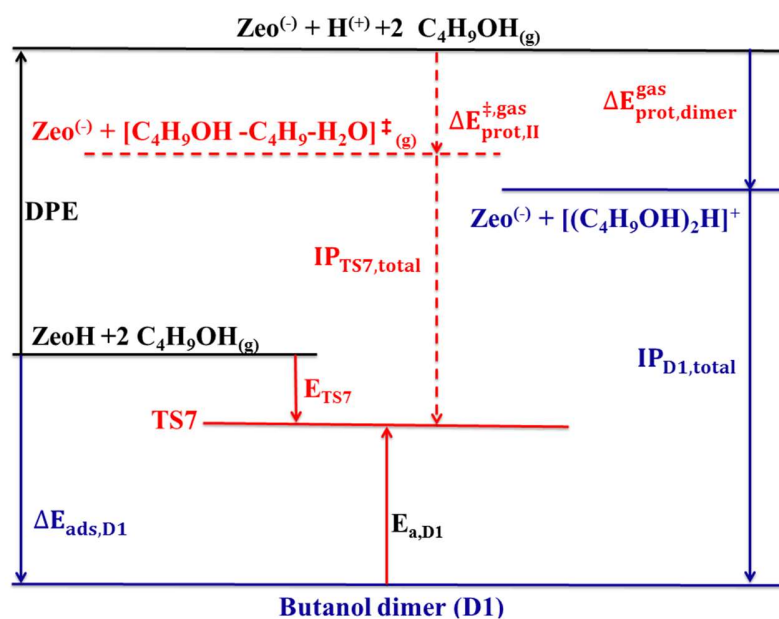


**Figure S4.** Thermodynamic cycle explaining the contributions to the adsorption ( $\Delta E_{ads,D1}$ ) and activation ( $E_{TS7}$ ,  $E_{a,D1}$ ) energies at 0 K for the butanol dimer D1 and the transition state TS7 in terms of zeolite deprotonation energy (DPE), protonation energy ( $\Delta E_{prot,dimer}^{gas}$ ,  $\Delta E_{prot,II}^{\ddagger,gas}$ ) and ion pair interaction energy ( $IP_{D1,total}$ ,  $IP_{TS7,total}$ ).

Adsorption of 1-butanol in the zeolite can be decomposed into the following thermodynamic cycle: i) deprotonation of zeolite, ii) gas phase protonation of butanol molecules to form protonated butanol dimer, iii) stabilization of the protonated butanol dimer within the zeolite framework. The adsorption energy at 0 K is given as

$$\Delta E_{ads,D1} = DPE + \Delta E_{prot,dimer}^{gas} + IP_{D1,total} \quad (1)$$

Here,  $\Delta E_{ads,D1}$  is the adsorption energy for the formation of adsorbed 1-butanol dimer (D1) from gas-phase 1-butanol at 0 K, DPE is the deprotonation energy of the zeolite,  $\Delta E_{prot,dimer}^{gas}$  is the gas-phase protonation energy ( $\Delta E_{prot,dimer}^{gas} = -913$  kJ/mol) for formation of protonated butanol dimer from two 1-butanol molecules calculated at the CBS-QB3 level of theory and  $IP_{D1,total}$  is the total ion-pair interaction energy between the protonated dimer and the zeolite framework.

Analogously, the 0 K energy for the formation of transition state TS7 from gas phase butanol,  $E_{TS7}$ , is composed of deprotonation energy (DPE), the energy for protonation and formation of a gas phase transition state analogue for TS7 from two 1-butanol molecules ( $\Delta E_{prot,II}^{\ddagger,gas} = -797$  kJ/mol) calculated at the CBS-QB3 level of theory and the stabilization energy of the transition state analogue within the zeolite framework ( $IP_{TS7,total}$ ).

$$E_{TS7} = \Delta E_{ads,D1} + E_{a,D1} = DPE + \Delta E_{prot,II}^{\ddagger,gas} + IP_{TS7,total} \quad (2)$$

The total interaction energy ( $IP_{D1,total}, IP_{TS7,total}$ ) is composed of dispersive ( $IP_{D1,D}/IP_{TS7,D}$ ) and non-dispersive ( $IP_{D1,DFT}/IP_{TS7,DFT}$ ) terms (Eqs. 3 – 6). The latter term consists of stabilizing electrostatic/hydrogen bonding interactions and a destabilizing distortion/steric constraints.

$$IP_{D1,D} = \Delta E_{ads,D1,D} \quad (3)$$

$$IP_{D1,DFT} = \Delta E_{ads,D1,DFT} - DPE - \Delta E_{prot,dimer}^{gas} \quad (4)$$

$$IP_{TS7,D} = E_{TS7,D} \quad (5)$$

$$IP_{TS7,DFT} = E_{TS7,DFT} - DPE - \Delta E_{prot,II}^{\ddagger,gas} \quad (6)$$

where  $\Delta E_{ads,D1,D}/E_{TS7,D}$  and  $\Delta E_{ads,D1,DFT}/E_{TS7,DFT}$  are DFT and dispersive contributions to the adsorption/activation energy at 0 K. Herein, dispersive contributions for the adsorbed intermediate and the transition state were obtained from DFT-D2 calculations using Grimme correction. The interaction energies for adsorbed dimer D1 and bimolecular transition state TS7 for different zeolites are listed in Table S5.

**Table S5.** Dispersive ( $IP_{D1,D}, IP_{TS7,D}$ ), non dispersive ( $IP_{D1,DFT}, IP_{TS7,DFT}$ ) and total ( $IP_{D1,total}, IP_{TS7,total}$ ) interaction energies ( $\text{kJ mol}^{-1}$ ) for adsorbed dimer D1 and bimolecular transition state TS7 In H-ZSM-5, H-ZSM-22 and H-FER.

	DPE <sup>a</sup>	Adsorbed dimer D1				Transition state TS7			
		$\Delta E_{ads,D1}$	$IP_{D1,total}$	$IP_{D1,DFT}$	$IP_{D1,D}$	$E_{TS7}$	$IP_{TS7,total}$	$IP_{TS7,DFT}$	$IP_{TS7,D}$
<b>H-ZSM-5</b>	1210	-283	-580	-407	-173	-155	-568	-400	-168
<b>H-ZSM-22</b>	1210	-288	-584	-404	-180	-155	-568	-376	-192
<b>H-FER</b>	1237	-259	-582	-362	-220	-116	-556	-329	-227

<sup>a</sup> deprotonation energies calculated using QM-Pot(MP2//B3LYP:GULP) [10]

A detailed insight is obtained by considering the individual contributing terms of the thermodynamic cycle. The gas phase proton affinity for the alcohol ( $\Delta E_{\text{prot,dimer}}^{\text{gas}}$ ) and the energy required for attaining the gas phase protonated TS analogue (from gas phase alcohol,  $\Delta E_{\text{prot,II}}^{\ddagger,\text{gas}}$ ) is a property of the alcohol species and the corresponding transition state and remains constant for all zeolites.

The deprotonation energy (DPE) is used for comparing the zeolite acid strength i.e. the lower the DPE the higher the acid strength. The H-FER zeolite has a relatively higher DPE value (1237 kJ/mol) in comparison to H-ZSM-5 and H-ZSM-22 (1210 kJ/mol).

The dispersive part of the interaction energy ( $IP_{D1,D}/IP_{TS7,D}$ ) increases with decreasing pore size from H-ZSM-5 < H-ZSM-22 < H-FER and is consistent with the literature reported trend for adsorption of primary alcohols in zeolites<sup>11,12</sup>. The dispersive stabilization of the transition state is comparable to the dispersive stabilization for the corresponding adsorbed reactant state, differing by at most 10kJ/mol (see Table S5), which can be attributed to their comparable sizes. On the other hand, the non-dispersive interaction energy ( $IP_{D1,DFT}/IP_{TS7,DFT}$ ) does not vary in the same manner (increasing in the order H-FER < H-ZSM-22 < H-ZSM-5 for D1 and TS7) and can be understood by considering its constituting terms. The non-dispersive interaction energy

( $IP_{D1,DFT}/IP_{TS7,DFT}$ ) term, is composed of stabilizing electrostatic/hydrogen bonding interactions and a destabilizing effect by distortion/steric constraints.

It is pertinent to note that unlike dispersive interaction which almost increases linearly with a decrease in pore size, the steric interactions tend to contribute significantly when the butanol molecules are very close to the zeolite surface or to each other.

Likewise, a thermodynamic cycle similar to that shown in Figure S5 was employed to analyze various contributing terms for the direct formation of 2t-butene from butanol dimer (D1). Again, as the pre-exponential factor does not vary significantly for this reaction, it allows to draw important conclusions based on the enthalpic contributions which in turn largely depend on the 0 K electronic energy obtained from the DFT calculations. The latter are used in the following analysis. The energy for protonation and formation of a gas phase transition state analogue for TS12 from two 1-butanol molecules,  $\Delta E_{prot,II}^{\ddagger,gas}$  is -786 kJ/mol calculated at the CBS-QB3 level of theory. The interaction energies for formation of 2t-butene from butanol dimer via transition state TS12 and the relative stability of TS12 w.r.t. D1 in different zeolites are listed in Table S6.

**Table S6.** Dispersive ( $IP_{D1,D}, IP_{TS7,D}$ ), non dispersive ( $IP_{D1,DFT}, IP_{TS7,DFT}$ ) and total ( $IP_{D1,total}, IP_{TS7,tot}$ ) interaction energies ( $\text{kJ mol}^{-1}$ ) for formation of 2t-butene from butanol dimer via transition state TS12 and relative stability of TS12 w.r.t. D1 in H-ZSM-5, H-ZSM-22 and H-FER.

	Transition state TS12				TS12-D1			
	$E_{TS12}$	$IP_{TS12, tot}$	$IP_{TS12, DFT}$	$IP_{TS12, D}$	$E_{TS12-D1}$	$IP_{TS12-D1, tot}$	$IP_{TS12-D1, DFT}$	$IP_{TS12-D1, D}$
<b>H-ZSM-5</b>	-76	-500	-341	-159	207	80	66	14
<b>H-ZSM-22</b>	-105	-528	-332	-197	183	56	72	-16
<b>H-FER</b>	-91	-542	-327	-215	168	40	35	5

As expected, the absolute value for the dispersive interaction energy increases with the decrease in pore size from H-ZSM-5 to H-FER (see  $IP_{TS12,D}$ ). Interestingly, the dispersive stabilization of the cationic TS12 fragment within these three zeolites does not follow the same trend as that for stabilization of D1 (as indicated by the relative dispersive interaction energies  $IP_{TS12-D1,D}$ ) with the straight channels of the 1-dimensional H-ZSM-22 providing much better dispersive stabilization for TS12 than the adsorbed D1 intermediate. This can be attributed to a combination of size and configuration of the complex within the different zeolite frame work.<sup>13</sup> The adsorbed dimer D1 on the other hand experiences a much higher stabilization by non-dispersive

interactions in comparison to TS12 (as seen from  $IP_{TS12-D1, DFT}$  of the Table 2 ). A comparison of the different zeolites indicates that the relative stabilization of TS12 w.r.t. D1 via non dispersive interactions ( $IP_{TS12-D1, DFT}$ ) increases from H-ZSM-5 to H-FER. A lower  $IP_{TS12-D1, DFT}$  (i.e. better stabilization of TS12 ) for H-FER can be attributed to a more significant electrostatic stabilization of the TS-12 in H-FER as compared to H-ZSM-5 (see Figure 5 in the main text for a qualitative comparison) and provides a possible explanation for the lower activation barrier for direct 2t-butene formation from D1 in H-FER.

### Comparison 1-butanol dehydration models

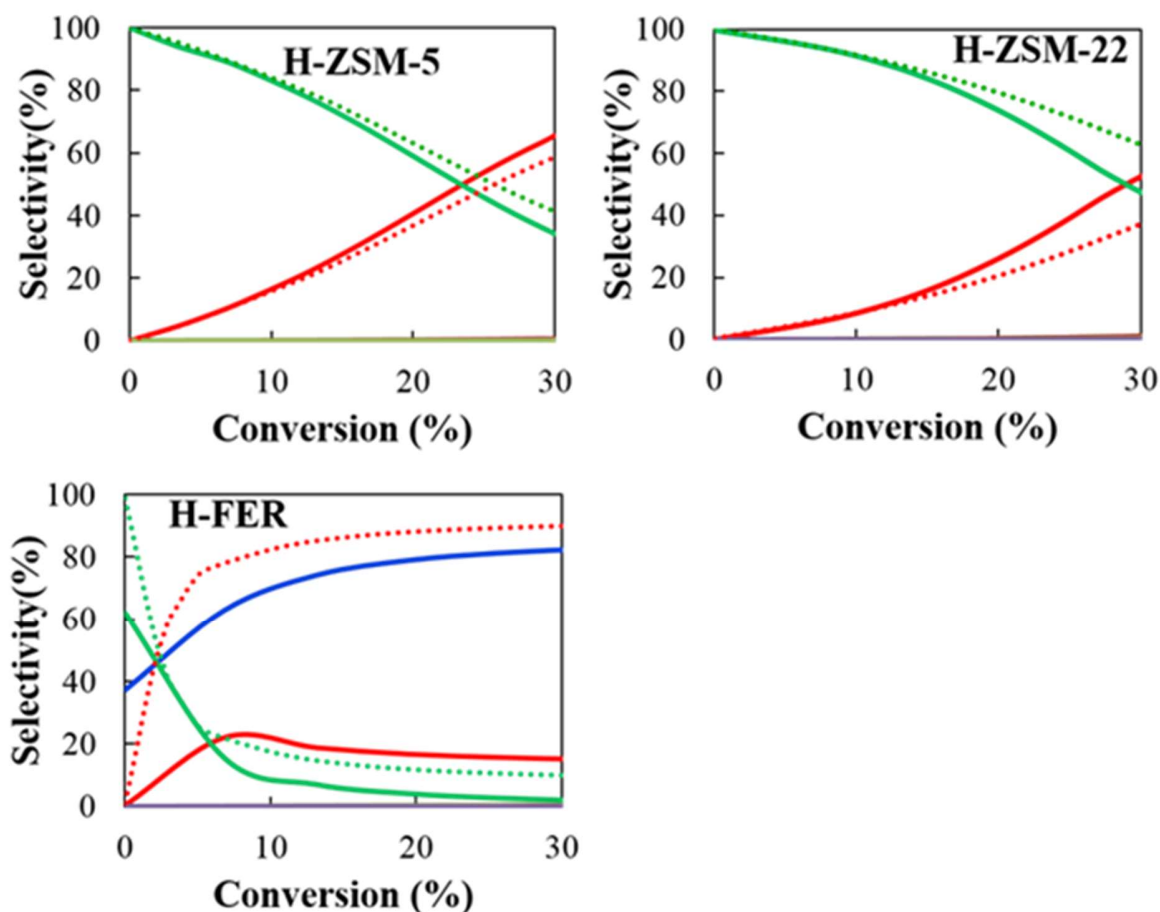


**Figure S5** : Simulated selectivity profile for formation of 1-butene  $\color{red}$   $\color{red}$ , 2t-butene  $\color{blue}$   $\color{blue}$ , 2c-butene  $\color{green}$   $\color{green}$  and DBE  $\color{purple}$   $\color{purple}$  for 1-butanol dehydration in different zeolites as a function of conversion at reaction temperature of 450 K and 1-butanol inlet partial pressure of 10 kPa. (The dotted and the bold lines refer to simulation results as obtained from previous work considering only dehydration of

butanol to 1-butene<sup>14</sup> and that obtained in the present study using the extended reaction network that includes the additional elementary steps that account for butene isomerization, respectively)

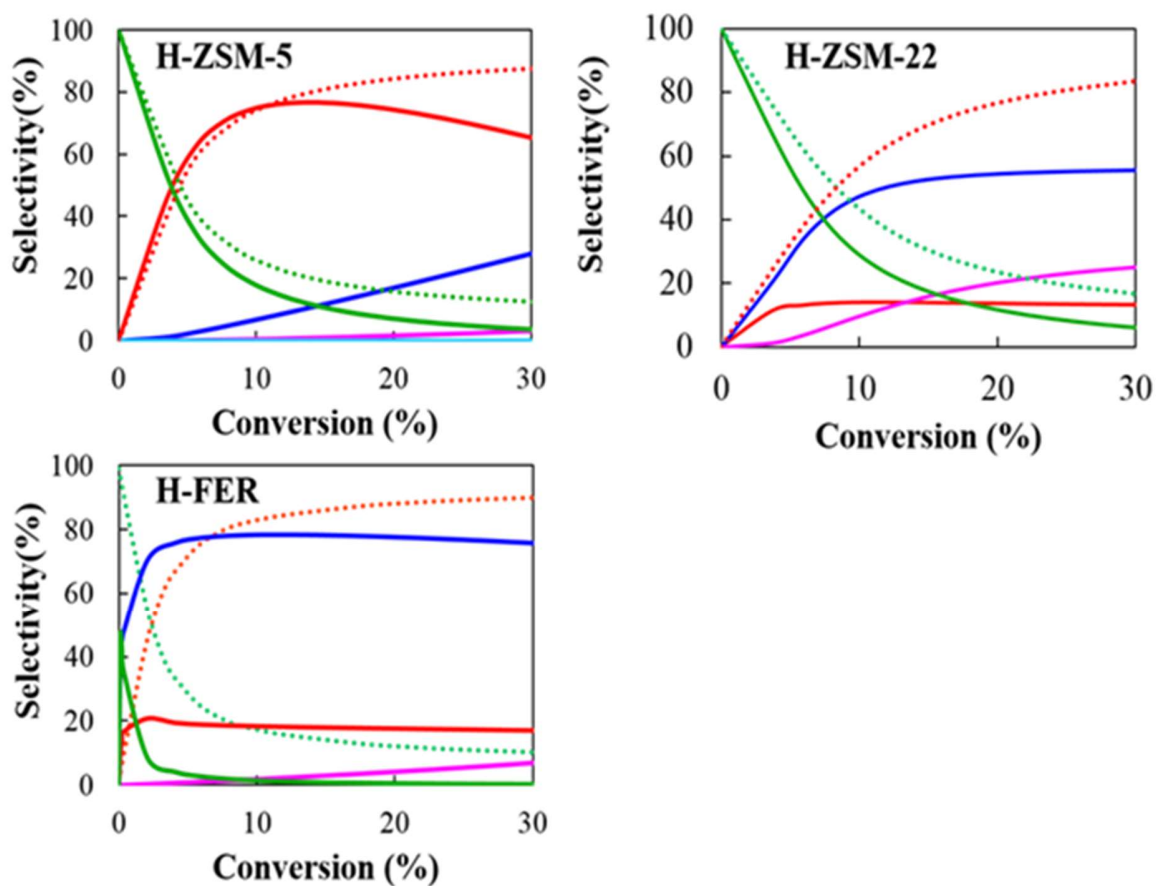


**Figure S6:** Simulated selectivity profile for formation of 1-butene —, 2t-butene —, 2c-butene — and DBE — for 1-butanol dehydration in different zeolites as a function of conversion at reaction temperature of **500 K** and 1-butanol inlet partial pressure of 10 kPa. (The dotted and the bold lines refer to simulation results as obtained from previous work considering only dehydration of butanol to 1-butene<sup>14</sup> and that obtained in the present study using the extended reaction network that includes the additional elementary steps that account for butene isomerization, respectively).

### Pressure dependency for 2-butene formation reactions:

A higher rate for the concerted double bond isomerization (mechanism  $m_{13}$ , Figure 14) in H-ZSM-22 ensures that the rate of formation of 1-butene remains the rate controlling step for the formation of 2-butenes during 1-butanol dehydration in H-ZSM-22. Therefore, the double bond isomerization reaction in H-ZSM-22 exhibits an initial zero order dependence ( $10^{-3} \leq P_{\text{BuOH},0} < 10^{-2}$  kPa), followed by a negative order dependence ( $10^{-2} < P_{\text{BuOH},0} < 1$  kPa) and then again a zero order pressure dependence ( $1 < P_{\text{BuOH},0} \leq 100$  kPa) according to the pressure dependence for the rate controlling path A mechanism  $m_4$  ( $10^{-3} \leq P_{\text{BuOH},0} < 1$  kPa) and path C mechanism  $m_9$  ( $1 < P_{\text{BuOH},0} \leq 100$  kPa). Meanwhile, four different regimes for 1-butanol pressure dependence are seen in the case of H-ZSM-5. In addition to the initial zero order ( $10^{-3} \leq P_{\text{BuOH},0} < 10^{-2}$  kPa), subsequent negative order ( $10^{-2} \leq P_{\text{BuOH},0} < 10^{-1}$  kPa) and later zero order ( $10^{-1} \leq P_{\text{BuOH},0} < 1$  kPa) butanol pressure dependence regimes (as seen in the case of H-ZSM-22), a fourth regime of negative order dependence is seen at butanol partial pressures above 1 kPa in the case of H-ZSM-5. The occurrence of such an additional regime is attributed to the decrease in the surface coverage of 1-butene and 2-butoxide with increase in butanol partial pressure (see Figure 13), making the TOF for 1-butene isomerization lower than the rate of formation of 1-butene via path C (see mechanism  $m_9$  vs. mechanisms  $m_{13}$ - $m_{15}$  in Figure 14). Thus, a decrease in TOF for double bond isomerization with increase in butanol partial pressure results in a net positive rate of formation of 1-butene and explains the increase in 1-butene selectivity in H-ZSM-5 at butanol partial pressures above 1 kPa, (corresponding to the fourth regime see Figure 13). The point of onset of the high butanol pressure negative order dependence regime in a zeolite is defined by

the butanol partial pressure at which the TOF for isomerization becomes lower than the TOF for formation of 1-butene. Overall, it is clear that a detailed insight into the butanol partial pressure dependence is needed in order to understand the cause for the differences observed in selectivity of butene isomers in different zeolites at high butanol partial pressures.

## References

- (1) Baerlocher, C.; Meier, W. M.; Olson, D.; Meier, W. M. *Atlas of zeolite framework types*; 5th rev. ed.; Elsevier: Amsterdam ; New York, 2001.
- (2) Dedecek, J.; Balgova, V.; Pashkova, V.; Klein, P.; Wichterlova, B. *Chem Mater* **2012**, *24*, 3231.
- (3) Dedecek, J.; Sobalik, Z.; Wichterlova, B. *Catal Rev* **2012**, *54*, 135.
- (4) Dedecek, J.; Lucero, M. J.; Li, C. B.; Gao, F.; Klein, P.; Urbanova, M.; Tvaruzkova, Z.; Sazama, P.; Sklenak, S. *J Phys Chem C* **2011**, *115*, 11056.
- (5) Nieminen, V.; Sierka, M.; Murzin, D. Y.; Sauer, J. *J Catal* **2005**, *231*, 393.
- (6) Wattanakit, C.; Boekfa, B.; Nokbin, S.; Pantu, P.; Limtrakul, J. *Abstr Pap Am Chem S* **2010**, 239.
- (7) Wattanakit, C.; Nokbin, S.; Boekfa, B.; Pantu, P.; Limtrakul, J. *J Phys Chem C* **2012**, *116*, 5654.
- (8) Gleeson, D. *J Mol Catal a-Chem* **2013**, *368*, 107.
- (9) Gleeson, D. *J Phys Chem A* **2011**, *115*, 14629.
- (10) Nguyen, C. M.; De Moor, B. A.; Reyniers, M. F.; Marin, G. B. *J Phys Chem C* **2012**, *116*, 18236.
- (11) Nguyen, C. M.; Reyniers, M. F.; Marin, G. B. *Phys Chem Chem Phys* **2010**, *12*, 9481.
- (12) Nguyen, C. M.; Reyniers, M. F.; Marin, G. B. *J Catal* **2015**, *322*, 91.
- (13) Herrmann, S.; Iglesia, E. *J Catal* **2017**, *346*, 134.

(14) John, M.; Alexopoulos, K.; Reyniers, M.-F.; Marin, G. B. *Acs Catal* **2016**, *6*, 4081.